# Computational Design of Stapled Peptide Inhibitor against SARS-CoV-2 Receptor Binding Domain

Asha Rani Choudhury, Atanu Maity, Sayantani Chakraborty, and Rajarshi Chakrabarti*

Department of Chemistry, Indian Institute of Technology Bombay, Powai, Mumbai-400076

E-mail: rajarshi@chem.iitb.ac.in

## Abstract:

Since its first detection in 2019, the Severe Acute Respiratory Syndrome Coronavirus 2 (SARS-CoV-2) has been the cause of millions of deaths worldwide. Despite the development and administration of different vaccines, the situation is still worrisome as the virus is constantly mutating to produce newer variants some of which are highly infectious. This raises an urgent requirement to understand the infection mechanism and thereby design therapeutic-based treatment for COVID-19. The gateway of the virus to the host cell is mediated by the binding of the Receptor Binding Domain (RBD) of the virus spike protein to the Angiotensin-Converting Enzyme 2 (ACE2) of the human cell. Therefore, the RBD of SARS-CoV-2 can be used as a target to design therapeutics. The α1 helix of ACE2 which forms direct contact with the RBD surface has been used as a template in the current study to design stapled peptide therapeutics. Using computer simulation, the mechanism and thermodynamics of the binding of six stapled peptides with RBD have been estimated. Among these, the one with two lactam stapling agents has shown binding affinity, sufficient to overcome RBD-ACE2 binding. Analyses of the mechanistic detail reveal that a reorganization of amino acids at the RBD-ACE2 interface produces favorable enthalpy of binding whereas conformational restriction of the free peptide reduces the loss in entropy to result in higher binding affinity. The understanding of the relation of the nature of the stapling agent with their binding affinity opens up the avenue to explore stapled peptides as therapeutic against SARS-CoV-2.

## Introduction:

The global pandemic caused by COVID-19 has been the cause of more than 4.8 million deaths as of October 2021 and has massively affected the global economy.[1] Several respiratory syndromes, pneumonia, etc. are caused by the infection of the SARS-CoV-2 (Severe Acute Respiratory Syndrome Coronavirus 2) and these are highly contagious in nature.[2,3] Although SARS-CoV-2 belongs to the same coronavirus family as MERS-CoV, SARS-CoV, etc.[4], the mutations have made the virus more resistant to neutralizing antibodies.[5] In addition to that, several new variants of the virus have been evolved which can escape the binding of antibodies, effective against the native form of the virus. The process of viral infection comprises several stages and different components of the virus are involved in these stages. In the very first step, the Spike protein of SARS-CoV-2 binds to the human ACE2 receptor.[6,7,8,9] The spike protein has a trimeric structure and each monomer is formed by several structural domains (Figure 1A).[10] During the virus attachment stage, the Receptor binding domain (RBD) of one monomer gets activated and attaches to the human ACE2 receptor followed by membrane fusion and internalization of genetic material.[11,12,13] A closer look at the RBD-ACE2 complex shows that the complexation is guided by the interaction of the α1 helix of ACE2 with the surface residues of the RBD.[14] The complexation eventually leads to the internalization of the virus and host membrane and the subsequent transfer of viral genetic material into the host cell. The attempts made to find the cure for this is designing vaccines, antibodies, and drugs that can inhibit the crucial stages of the infection process. The continuous effort to suitable inhibitor molecules which can be used as drugs to target different proteins of the virus e. g. the main protease (MP), non-structural proteins (NSP) domains, receptor-binding domain (RBD), etc. Among these, RBD has been targeted most because of its direct interaction with the human ACE2 receptor. Unlike the other targets, the protein-protein interaction interface between ACE2 and RBD is quite extended and flexible,[15] thereby designing an inhibitor is challenging.[16]

The two most widely used classes of inhibitors are small molecules and peptides.[17,18] Due to the wide shape of the binding pocket, small molecule inhibitors often lack specificity against wider binding pockets like that of RBD.[19] Rather a peptide inhibitor is more suitable to target such kind of interface.[20] There are few efforts to design peptide inhibitors against ACE2. The basic working principle is to design a peptide that can mimic the binding mode of ACE2 with RBD. The simplest possible solution is to use the alpha helix of ACE2 which binds to RBD as a potential inhibitor. However, the wildtype α1 helix of ACE2 has been reported to lack proper binding with RBD in previous studies.[21] This has led to a modification of the wild-type peptide

yielding new peptides. These modifications mainly include mutation of some non-essential amino acids, use of crosslinkers to enhance binding affinity. Amino acids at suitable positions along the peptide backbone can be replaced with a specific functional group which can be further crosslinked to generate stapled peptides.[22,23] Stapled peptides have shown promising results to inhibit different protein-protein interactions. By altering the length, attachment point, and chemical nature of the stapling agents, the design of stapled peptides can be tuned to achieve desirable affinity and target specificity.[18,24,25] Few experimental and computational reports have checked the stability of stapled ACE2 and their binding with RBD.[21,26,27] However, a rationale to combine stapling agents chemical nature and length with their binding affinity is still lacking which is crucial for the future design of stapled peptides.

In the current work, we have considered aliphatic and lactam stapling agents and used a combination of them to design four stapled peptides. Binding free energy calculation from extensive molecular dynamic simulation for the binding of stapled and unstapled peptides reveals that the binding is guided by both gain in enthalpic interaction and loss in entropic penalty. The staple ACE2 peptide, with two i-i+4 lactam staples, is found to exhibit the most favorable binding.

## Methods:

### Computational design of peptide inhibitor:

The structure of RBD bound to the α1 helical domain of ACE2 is modeled starting from the complex of SARS-CoV-2 RBD and full-length human ACE2 (PDB ID: 6M0J)[7]. From the crystal structure, 25 residues (21 to 45) of full-length α1 (21 to 56) are found to be involved in effective interaction with the RBD binding pocket residues. This 25-residue domain ($I^{21}$EEQAKTFLDKFNHEAEDLFYQSSL$^{45}$) is chosen as our starting peptide (termed as ACE2_wt (wild type ACE2)) in the rest of the manuscript) and modified further to design other peptides. The truncated form of α1 have been found to effectively bind RBD in some previous studies.[28,29,30] The residues of α1 helix of hACE2 which interact favorably with RBD binding pocket are Gln24, Tyr27, Asp30, Lys31, His34, Glu35, Glu37, Asp38, Tyr41, and Gln42.[31,32] Thus, our approach is to design high-affinity 25-mer peptide inhibitors where these residues will not be altered.
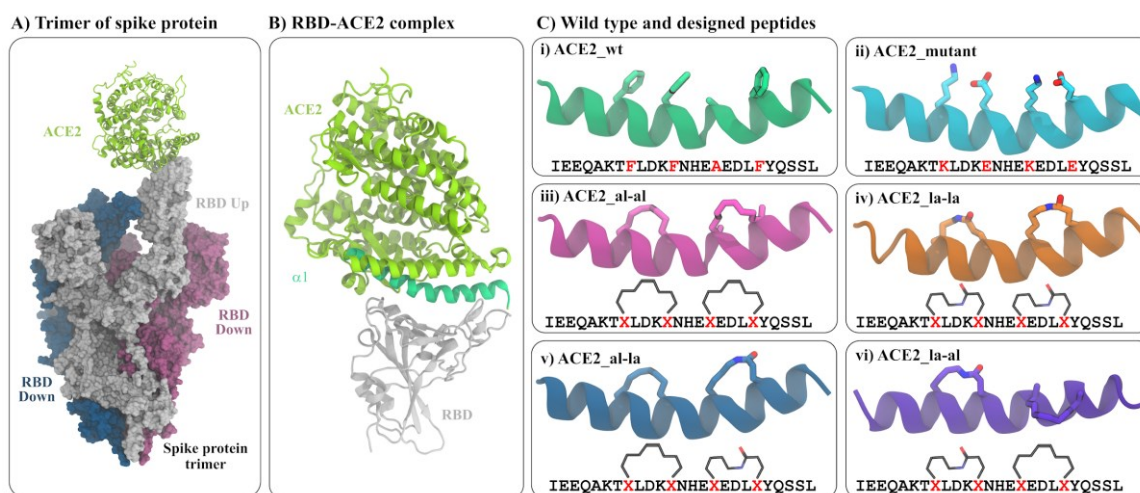
**Figure1:** Modeling of the RBD-ACE2 interaction. (A) The trimeric assembly of SARS-CoV-2 spike protein in complex with human ACE2 protein. Out of three spike proteins, two (blue and red surface) have their RBD buried (RBD Down) and one (white surface) is with an exposed RBD (RBD Up) conformation which binds at one end of human ACE2 (light green cartoon). (B) ACE2 interacts with amino acids of RBD (white ribbon) through its α1 helix (green ribbon). (C) The structures and sequences of the truncated α1 and five modified peptides. The amino acids at positions 28, 32, 36, and 40 are shown in sticks. The details of mutation and attachment of stapling agents are listed in Table1.

In this work, we have used a stapling approach where the side chains of two amino acids of ACE2_peptide are joined together to form a stapled peptide.[22,23] and their binding with RBD is investigated. Since α1 of ACE2 binds in helical conformation, the helical propensity of the designed peptide will be crucial in binding with its target partner RBD of SARS-CoV-2.[31] Hence, for a large peptide of 25 residues, two i-i+4 staples will be more useful than a single i-i+7 staple in maintaining its helical structure. The stapling positions are selected based on the conditions that replaced residues should not be among those residues which have favorable interactions with RBD as previously reported[31,32] and the newly designed peptides should have the proper orientation to gain a stronger binding affinity to RBD.[29] Considering all these above facts, we have selected our stapling positions by replacing Phe28, Phe32 to form an i-i+4 staple and another i-i+4 staple in the positions of Ala36 and Phe40. Two stapling agents are considered as crosslinkers between the two pairs of residues one of which is an all-hydrocarbon staple and the other is a lactam crosslinker. A combination of these two stapling agents is used to design four stapled peptides. A peptide with mutations at the aforementioned four positions (F28K, F32E, A36K, and F40E) is also designed. The details of these peptides and their complex with RBD are listed in table 1.

***Simulation Details:***

The CHARMM36[33] forcefield parameters are employed to design the protein-peptide complex and a combination of CHARMM parameters of proteins and small molecules (CGENFF) are

used to model the two stapling agents. For designing an aliphatic crosslinker at targeted i and i+4 residues position, first, the amino acids are replaced by lysine group and then s-NH2 groups of lysine are replaced by an aliphatic chain having an olefinic bond, and end of the two aliphatic side chains are joined together,[34] whereas for ACE2_mutant, i and i+4 residues are mutated to lysine (K) and glutamic acid (E) and for lactam crosslinker designing these mutating residues are patched together to form am -C(O)-NH linkage.[27] This strategy has been successfully used to model stapled peptides in other studies as well. Taking all these cross-linker designs into account, we have modeled 4 types of stapled versions of ACE2_wt, first one is ACE2 with a double aliphatic crosslinker (abbreviated as ACE2_al-al) where one staple is at 28 – 32 residue and another at 36 – 40 position, the second one is ACE2_wt with double lactam crosslinker (abbreviated as ACE2_la-la) where two staples are at 28 – 32  and 36 – 40 position, the third one is  ACE2_wt with one aliphatic and one lactam staple (abbreviated as ACE2_al-la) where aliphatic liker is at 28 – 32 and lactam linker is at 36 – 40 and the last one is vice versa of the previous one that is lactam is at 28 – 32 and aliphatic is at 36 – 40 position (abbreviated as ACE2_la-al). Along with all these designed peptides, 25-mer ACE2 (abbreviated as ACE2_wt) and a mutated version of ACE2_wt (ACE2_mutant) are considered for a better structural comparison and their binding with RBD. All the 6 peptides are simulated in the free state and in complex with RBD.  Also, only the RBD is simulated for the calculation of binding energy following the multiple trajectory approach.

**Table 1:** Details of the system compositions and simulation lengths for different systems.

| | System Identifier | Protein | Peptide | Simulation length |
|---|---|---|---|---|
| 1 | ACE2_wt | -- | Truncated α1 helix of ACE2 (21 to 45) | $3 \times 1\,\mu S$ |
| 2 | ACE2_mutant | -- | ACE2_wt with F28K, F32E, A36K, and F40E mutations | $3 \times 1\,\mu S$ |
| 3 | ACE2_al-al | -- | ACE2_wt with two i-i+4 aliphatic staples between residue pairs 28, 32 and 36, 40 | $3 \times 1\,\mu S$ |
| 4 | ACE2_la-la | -- | ACE2_wt with two i-i+4 lactam staples between residue pairs 28, 32 and 36, 40 | $3 \times 1\,\mu S$ |
| 5 | ACE2_al-la | -- | ACE2_wt with one i-i+4 aliphatic staples between residue pairs 28, 32 and one lactam staple between residue pairs 36, 40 | $3 \times 1\,\mu S$ |
| 6 | ACE2_la-al | -- | ACE2_wt with one i-i+4 | $3 \times 1\,\mu S$ |

| | | | lactam staples between residue pairs 28, 32 and one aliphatic staple between residue pairs 36, 40 | |
|---|---|---|---|---|
| 7 | RBD | SARS Cov2 Receptor Binding domain (Residues # to #) | -- | $3 \times 1\,\mu S$ |
| 8 | RBD + ACE2_wt | RBD | ACE2_wt | $3 \times 1\,\mu S$ |
| 9 | RBD + ACE2_mutant | RBD | ACE2_mutant | $3 \times 1\,\mu S$ |
| 10 | RBD + ACE2_al-al | RBD | ACE2_al-al | $3 \times 1\,\mu S$ |
| 11 | RBD + ACE2_la-la | RBD | ACE2_la-la | $3 \times 1\,\mu S$ |
| 12 | RBD + ACE2_al-la | RBD | ACE2_al-la | $3 \times 1\,\mu S$ |
| 13 | RBD + ACE2_la-al | RBD | ACE2_la-al | $3 \times 1\,\mu S$ |
| | | | | $39\,\mu S$ |

The N-terminal and C-terminal amino acids of RBD and ACE2-peptides in the free and bound states are capped with acetyl and amide group respectively to avoid unwanted interaction of the bare terminal charges with rest of the system. Each of the systems is neutralized by adding the required numbers of $K^+$ and $Cl^-$ ions and solvated in a cubic water box made of TIP3P water,[35] where the size of the box is determined by maintaining a distance of at least 1 nm between the water box edge and protein/peptide atoms to satisfy the periodic boundary condition. For the removal of initial steric clashes, a 5000-step energy minimization is performed for each system using the steepest descent method.[36] Subsequently, a 500 ps equilibration in the NVT ensemble is performed to equilibrate each system at 310K to avoid void formation in the box followed by a 20ns equilibration at isothermal- isobaric (NPT) ensemble to attain a steady pressure of 1 atm considering a pressure relaxation of 1ps. The temperature is kept constant at 310 K by applying the V–rescale thermostat[37] and the pressure was maintained to be at 1 atm using Parrinello-Rahman barostat[38] with a pressure relaxation time of 2 ps, used for the attainment of desired pressure for all simulations. Finally, the production runs for 1000ns with a time step of 2 fs, are performed. All the simulations are performed in GROMACS.[39] Short-ranged Lennard–Jones interactions are calculated using the minimum image convention.[40] For estimating non-bonding interactions including electrostatic as well as van der Waals interactions, a spherical cut-off distance of 1 nm is chosen. Periodic boundary conditions have been used in all three directions to remove edge effects. SHAKE algorith[41] is applied to constrain bonds involving the hydrogen atoms of the water molecules. Long-range electrostatic interactions are calculated using the particle mesh Ewald (PME) method.[42] The frames in the trajectory are saved at a frequency of 2 ps for analyses. To extract different structural properties and for visualization, in-built modules of

GROMACS,[39] VMD[43], and some in-house scripts are used.

***Binding energy calculation:***

The most popular and comparably less computationally expensive method MM-GBSA (molecular mechanics with the generalized bond surface area) is used to calculate the standard free energy of binding ($\Delta G$). Generally, the binding free energy of a protein–peptide complexation is calculated by subtracting the free energy of both protein and peptide in their free state from the free energy of the protein-peptide complex.[44]

$$\Delta G = G_{complex,\ solvated} - [\ \Delta G_{protein,\ solvated} + \Delta G_{\ peptide,\ solvated}] \tag{1}$$

where $\Delta G_{solvated}$ can be represented as,

$$\Delta G_{solvated} = E_{gas} + \Delta G_{solvation} - TS_{solute} \tag{2}$$

which can further can be simplified as -

$$\Delta G_{solvated} = E_{internal} + E_{vdw} + E_{elec} + E_{polar\ solvation} + E_{nonpolar\ solvation} - TS_{solute} \tag{3}$$

The first three terms of equation (3) describe the gas-phase energy which arises due to molecular motion such as bond vibration, angle bending, dihedral rotation, etc., and Vander Waal and electrostatic interaction respectively. The fourth and fifth terms represent the solvation free energy calculated considering implicit environments in two separate parts, i.e., polar and non-polar components. The polar solvation energy is estimated considering GB (Generalized Born) solvent model and the nonpolar component is assumed to be proportional to the solvent accessible surface area (SASA).[45,46] The last term is solute entropy, where T represents the absolute temperature and S is the entropy of the solute, whereas the solvation entropy is already incorporated in solvation energy terms.[47] The solute entropy is calculated by considering quasi-harmonic approximation.[48] In short, the sum of the first five terms is considered as enthalpy, H although it includes the solvation entropy term and simply can be written as,

$$\Delta G = \Delta H - T\Delta S \tag{4}$$

In practice, all the simulations of the free and complex state are performed in explicit water to get the conformational microstates of the solute, and then the free energy of solvation of these conformations are estimated using an implicit environment after the removal of explicit water molecules. In this work, we have followed multiple trajectory protocols (MTP) and performed three independent simulations of RBD+ACE2_wt, modified RBD+ACE2_wt systems, RBD

and ACE2, and their mutant and stapled versions. All of the free energy of solvation and entropy calculation is performed in CHARMM[49] and averaged over 50000 conformations of each system over the last 500 ns of the simulations. The values calculated for the three simulations are summarized in Supplementary material Tables (Table S1 – S19) and an average of the three simulations is provided in Table 2.

## Results:

### *The dynamics of the N-terminal loop of RBD is regulated by ACE2-peptide binding*

The binding of ACE2 and RBD is governed by mainly electrostatic interaction between the residues of the binding pocket of RBD and the α1 helix of ACE2.
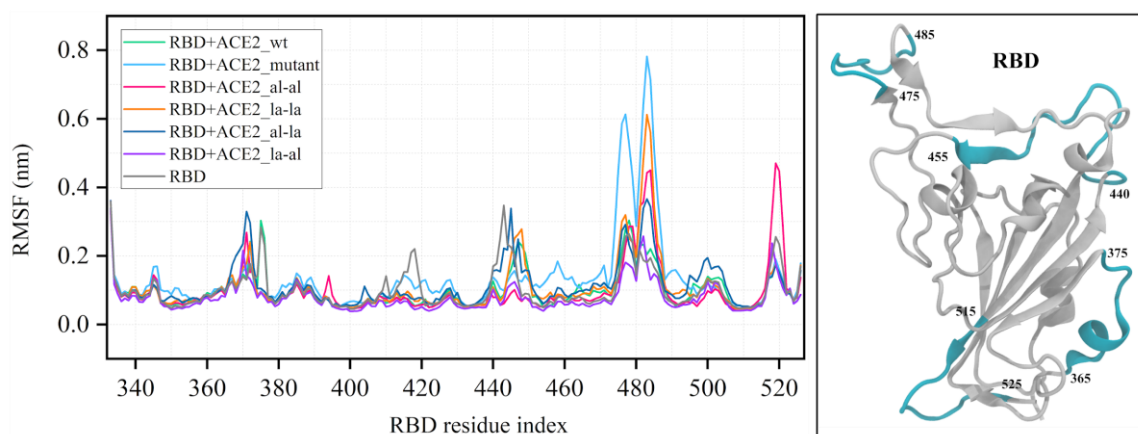


**Figure 2:** Root mean square fluctuation (RMSF) of the receptor-binding domain (RBD) in a bound state with different designed peptides. For system identification, the color of the graph line and system name is maintained in the above plot. The right-hand side figure indicates RBD in its free state and its different loops.

To compare the structural changes in RBD induced by ACE2_wt peptide and other designed peptides, the root mean square fluctuation of the residues of RBD was calculated. The RMSFs of the amino acids of RBD in the presence of different peptides and the absence of them are plotted in Figure 2.  The fluctuations in different regions of RBD vary when different peptides interact with the binding pocket residues. Maximum fluctuation is observed in the residue range 470 to 490 which belongs to the loop region close to the ACE2 binding pocket of RBD. The higher fluctuations in that region in the presence of peptides are a reflection of the direct interaction of the loop residues with the peptides. The interaction of the loop residues with ACE2 peptides was quantified by using a contact map between the residues of the two regions (Figure S1). From the plot, it is clear that there is a significant enhancement of the contacts between the two structural regions when the ACE2-peptide is modified by mutation or by

adding stapling agents. Since the stapling agents modify the peptide conformations, the interaction of ACE2-peptides with the binding pocket residues of RBD will also be altered. A qualitative description of that has been provided as a representative snapshot of the three ACE2-peptides in Figure 3.
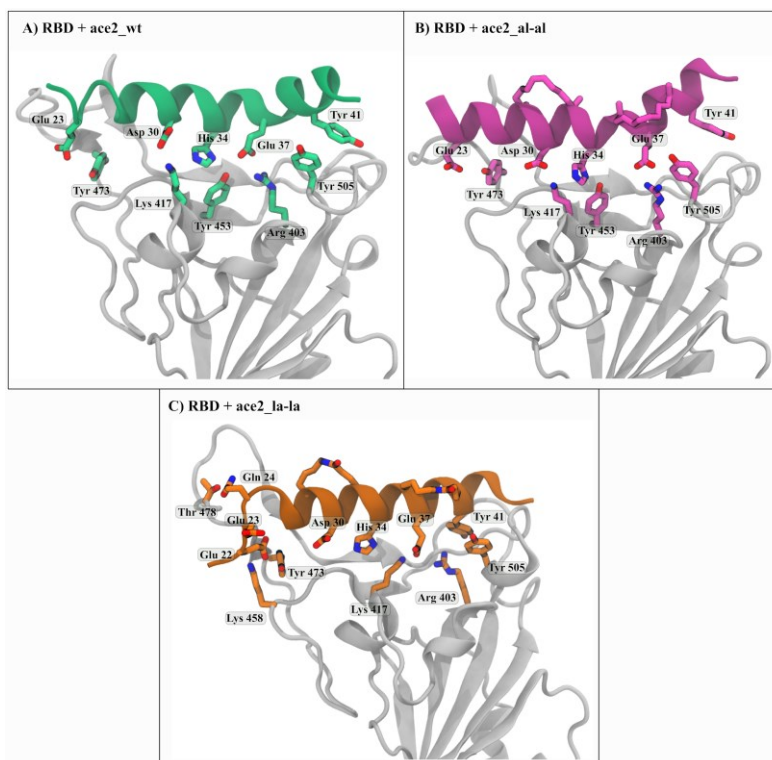


**Figure 3:** Residue level interaction between Receptor binding domain (RBD) and (a) 25-mer ACE2_wt, (b) ACE2 with double aliphatic crosslinker (ACE2_al-al) and (c) ACE2 with double lactam crosslinker (ACE2_la-la).

The ACE-2 peptide is stabilized on the binding pocket of RBD mainly by polar interaction between the amino acids (Glu23, Asp30, His34, Glu37, Tyr41) of RBD facing side of ACE-2 peptide and the amino acids (Tyr473, Lys 417, Tyr 453, Arg403 and Tyr505) at the surface of RBD. The interacting amino acids of ACE2_wt and RBD are shown in Figure 3a. The interacting residues get reorganized and that modifies the interaction between the peptide and RBD. The extent of this alteration is different in the presence of different kinds of stapling agents. For example, the interactions are slightly modified between RBD and ACE2_al-al (Figure 3b) whereas there is a significant change in the peptide conformation in RBD+ACE2_la-la and that involves more RBD residues in interaction (Figure 3c).

The structural rearrangements in both ACE2-peptide and RBD will impact the ACE2-peptide-RBD binding process and this can be quantified by calculating their binding free energies. The

binding free energy is calculated using MMGBSA protocol as it is found to be a considerably accurate yet computationally less expensive method for binding energy estimation.[34,50,51]

*Binding Energy Governed by Both Enthalpy and Entropy:*

The binding free energies are estimated for RBD bound to six ACE2-peptides. The average binding free energy was quantified considering both enthalpy and entropy. The enthalpy was calculated using the MMGBSA protocol, a formalism used to find the solvation energy using a continuum model of implicit solvent. The conformational entropy is estimated considering quasi-harmonic approximation on the ensemble of conformations. These values are calculated over the last 500 ns of 1μs trajectory and further averaged over the three independent simulations for each peptide. The results are summarized in Table 2.

**Table 2:** Components of binding free energy of RBD-ACE2-peptide binding. All energy values are in kcal/mol.

| Energy components | RBD + ACE2_wt | RBD + ACE2_mutant | RBD + ACE2_al-al | RBD + ACE2_la-la | RBD + ACE2_al-la | RBD + ACE2_la-al |
|---|---|---|---|---|---|---|
| $\Delta E_{Elec}$ | -273.05 | -272.86 | -294.54 | -285.80 | -215.85 | -349.18 |
| $\Delta E_{vdw}$ | -30.74 | -38.03 | -45.65 | -47.43 | -30.50 | -41.44 |
| $\Delta E_{internal}$ | 19.77 | -0.98 | -0.36 | -0.57 | -2.23 | 3.05 |
| $\Delta E_{solv(polar)}$ | 245.30 | 262.66 | 288.16 | 272.07 | 209.51 | 336.51 |
| $\Delta E_{solv(non-polar)}$ | -1.60 | -2.28 | -2.89 | -3.25 | -1.89 | -2.65 |
| $\Delta E_{Elec+solv(polar)}$ | -27.75 | -10.2 | -6.38 | -13.73 | -6.34 | -12.67 |
| $\Delta H$ | -40.31 | -51.50 | -55.28 | -64.98 | -40.96 | -53.72 |
| $-T\Delta S$ | 21.97 | 27.83 | 28.67 | 19.08 | 6.08 | 31.74 |
| $\Delta G$ | -18.34 | -23.67 | -26.61 | -45.90 | -34.88 | -21.98 |

From the binding energy values, it is clear that most of the ACE2 peptides with the stapling agent or with mutation show favorable binding affinity with RBD of SARS-CoV-2. Out of six ACE2 peptides and their stapled versions, ACE2 with lactam double crosslinker (ACE2_la-la) shows the best binding affinity value (~ -46 kcal/mol). A direct comparison of the binding energy values with the experimental binding energy is not possible as that is not available for a peptide with the exact same sequence. However, a 30-residue peptide derived from ACE2 (TIEEQAKTFLDKFNHEAEDLFYQSSLASWN) has shown a binding affinity of -5.71 kcal/mol and a stapled version of it with two aliphatic staples has affinity -7.81 kcal/mol.[21] A comparison of the binding of another ACE2-α1-derived peptide (IEEQAKTFLDKFNHEAEDLFYQSSLASWNYNTNIT) and its variant with one lactam staple has shown significantly improved binding for the stapled one.[27] Although a quantitative comparison of the experimental binding energy and that calculated from this study is not

possible, the relative binding affinity of an unstapled and stapled peptide with RBD calculated here agrees well with the experimental findings. A comparison of both enthalpy and entropy values for different peptides reveals that the stapling agents not only reduce the entropic cost of complexation but also enhance the enthalpy of binding. Interestingly, both enthalpy and entropy contribute to the binding energy value as for enthalpy, polar interactions play a very important role whereas conformational flexibility of peptide both in free state and complex bound state contributes to the entropy.

By mutating some hydrophobic and non – interacting residues of ACE2_wt with polar residues such as lysine and glutamic acid, there is a sharp increase in the value of polar solvation energy is noticed for RBD+ACE2_mutant system. Since, for RBD+ACE2_la-la these mutated polar residues are patched together to form lactam crosslinker, so here also protein-peptide and peptide-solvent polar interaction are developed which is reflected in their electrostatic and polar solvation energy values. Also, this effect is observed in designed staples having lactam groups such as RBD+ACE2_la-al but not in the case of RBD+ACE2_al-la. Exceptionally, in the case of RBD+ACE2_al-al, despite using a hydrophobic chain as a crosslinker, polar interactions have developed. Generally, electrostatic and polar solvation energy terms are complementary to each other i. e. if there is a gain in the electrostatic energy upon binding it is usually associated with a loss in the polar solvation energy because the protein-solvent polar interactions for the residues forming the binding interface are replaced by the protein-protein electrostatic interactions. However, due to the replacement of polar residues as a stapling agent, both the values increase simultaneously and result in a favorable enthalpy value. In addition to this, there is also a 15 to 17 kcal/mol increasing van der Waals energy particularly for RBD+ACE2_al-al and RBD+ACE2_la-la which eventually contribute to the enthalpy value. All these changes in the enthalpy and entropy values can be correlated with the molecular level protein-peptide interaction and conformational switching from the free to a bound state of the peptides. These two have been quantified in detail in the following sections.

### Stapling induces polar amino acid-mediated interaction

A sum of electrostatic and van der Waal interactions of each amino acid of ACE2-peptides with the RBD residues has been calculated and plotted in figure 4. For all of the peptides, there is a net increase in interaction energy value compared to that in the RBD+ACE2_wt. Interestingly, the addition of stapling agents to positions 28, 32, 36, and 40 enhances the interaction energy of residues facing the binding pocket of RBD, mainly Glu23, Asp30, and

Glu37 (Figure 4A). These aspartates and glutamates with acidic side chains are well known to form several polar interactions with other amino acids containing polar side chains. The most common interaction is forming a salt bridge interaction with amino acids having positively charged side chains i. e. Arginine and Lysine. RBD contains a few such residues in its binding pocket, for example, Arg403, Lys417, Lys458. The distances between the residue pairs forming effective salt-bridge interaction are plotted throughout the simulation for different systems (Figure 4C). A typical salt bridge interaction is formed when the distance between any of the oxygen atoms (O) of an acidic amino acid side chain from the nitrogen (N) of any basic amino acid side chain is less than 0.4 nm.[52] For the RBD+ACE2_wt system, the distances for salt bridges Lys31-Glu484, Asp38-Lys403, Gly37-Lys417 are found to be greater than 0.4 nm during the simulation time (Figure 4C). However, the residue pair Asp30-Lys417 are found to be in a favorable distance to form stable salt bridge interaction. Interestingly in the RBD-stapled ACE2-peptide complexes, some of these residue pairs satisfy the distance criteria and form stable salt-bridges interaction (Figure 4C). For example, Glu23 and Lys485 form strong salt bridges in RBD+ACE2_mutant and RBD+ACE2_al-la system whereas Asp30 and Lys417 are at a favorable distance for salt bridge interaction in RBD+ACE2_al-al and RBD+ACE2_al-la systems.
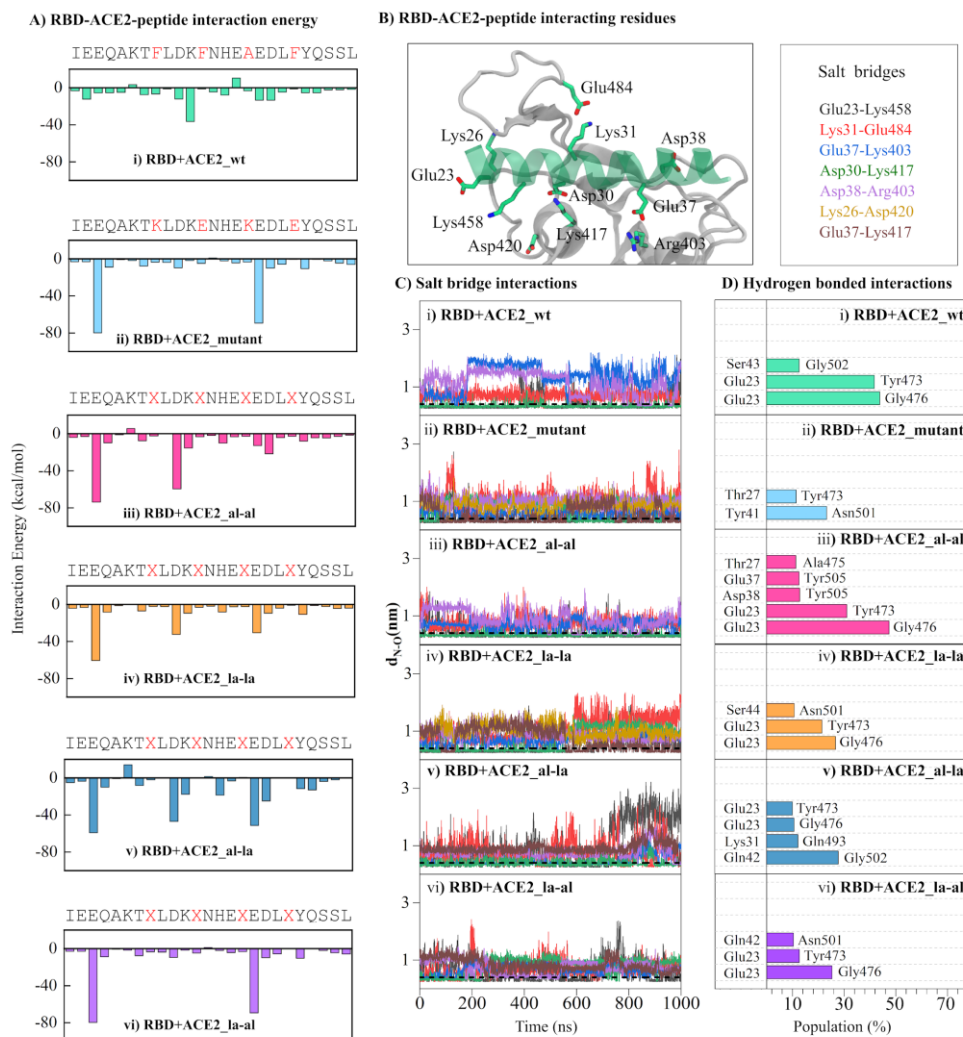
**Figure 4**: RBD-ACE2 interactions: (A) The average interaction energy (as a sum of electrostatic and van der Waals energy) of each ACE2-peptide residue with the binding pocket residues of RBD. The residues mutated or replaced by stapling agents are shown in red in the ACE2 sequence. (B) The amino acids of ACE2 (green transparent ribbon) and RBD (white ribbon) involved in salt-bridge interaction are shown in stick representation. The carbon, nitrogen, and oxygen atoms are colored green, blue, and red respectively. The residue pairs forming effective salt-bridge interaction are listed in the right-hand side box. (C) The distances ($d_{N-O}$) between any of the oxygen atoms of Glu/Asp with the nitrogen atom of respective Lys/Arg for the salt-bridge pairs listed in (B) are plotted for different systems. The horizontal black dotted line at $d_{N-O} = 0.4$nm represents the cutoff for effective salt-bridge formation. (D) The populations of hydrogen bonds formed between ACE2 and RBD residues are shown for different systems. The population is calculated as the percentage of simulation time the pairs form a successful hydrogen bond.

In addition to these salt-bridges several new hydrogen-bonded interactions have been developed between RBD and modified ACE2 peptides (Figure 4D). The occupancies of the significant hydrogen bonds are shown in the plot and the corresponding molecular level pictures showing these interactions are presented in Figure S2. Both these two types of polar interactions have contributed to the improved enthalpic contribution to the binding energies. Some of the resiudes involved in important interactions

have been found to be crucial for RBD-ACE2 binding and effect of their mutation have influenced the RBD-ACE2 binding.[53]

*Conformational restriction by stapling agent contributes to entropic stabilization*

The quantity of changes in entropy in the process of complex formation by combining two moieties depends on their entropy in the free and bound state. In the biomolecular complexation process like the one studied here, this entropy is usually the conformational entropy and is directly related to their conformational fluctuation. Since peptides are more flexible in their free state compared to in complex with protein, the entropy of protein-peptide binding is usually negative. Stapled peptides are known to reduce this entropic penalty by inducing conformational restriction to the free peptide.[34] The fluctuations of the peptides in their free and the RBD-bound state have been compared by calculating two properties, root mean square fluctuation (RMSF) of peptide residues and the helical propensity of the peptides.

The RMSFs of the 25-residue peptides are plotted both in their free state and in their complex with RBD in figure S3. From the values range of RMSF it is evident that the fluctuation gets reduced in the complexed state (Figure S3B) compared to their free state (Figure S3A). In the free state, the introduction of two lactam staples (ACE2_la-la) reduces the fluctuation quite significantly. For other stapling agents also, there are considerable decreases in RMSF values compared to ACE2_wt except for ACE2_al-al and ACE2_mutant which shows higher RMSF especially towards the C-terminal end of the peptide (residues 32-45) (Figure S3A). In the RBD-bound state, all of the peptides show reduced RMSF compared to RBD+ACE2_wt representing a favorable binding in the RBD binding pocket. The only exception is the system where the aliphatic stapling agent was added (RBD+ACE2_al-al) which shows higher fluctuation even in the complexed state. Although these comparisons provide an understanding of the relative stability of the peptides in the free and RBD-bound state, the fluctuations of the same peptide in the free and RBD-bound state have to be compared to find the difference in fluctuation which can be accounted for the entropy of binding. This comparison for each peptide is presented in Figure 5.
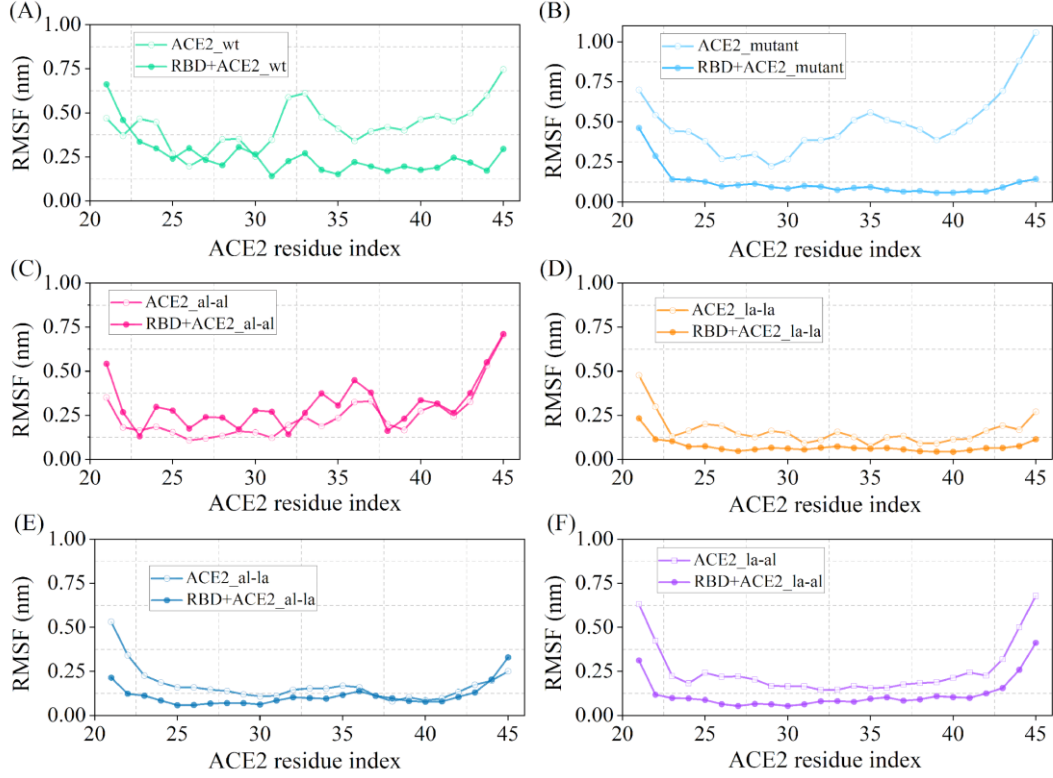
**Figure 5:** Comparison of RMSF values of wild-type ACE2 and stapled peptides in the free state and bound state.

If there is a considerable overlap between the RMSF of the residues of ACE2-peptide in the free and RBD bound state that will require less conformational reorientation during binding hence the process will be associated with a smaller decrease in entropy. The two plots (free and complexed) deviate significantly for ACE2_mutant (Figure 5B) and ACE2_al-al (Figure 5C) compared to that in ACE2_wt (Figure 5A). This leads to an increase in the entropic penalty to ~28 kcal/mol and ~29 kcal/mol compared to ~22 kcal/mol for ACE2_wt (Table 2). Since the overlap has improved in the case of ACE2_la-la (Figure 5D) and ACE2_al-la (Figure 5F) from ACE2_wt, the associated change in entropy has been reduced to ~19 kcal/mol and ~6 kcal/mol respectively.

The ACE2 peptide forms complex with RBD in a helical conformation to fit into the binding pocket and also to maximize polar interactions with the RBD residues. Therefore, the helical propensity of the peptides will also play a key role in determining the binding thermodynamics. The helical fraction of peptide is calculated using formula implemented in PLUMED[54]. First the number of six residue α- helical stretches (S) in peptide is calculated using formula[55]:

$$S = \sum_\alpha n[RMSD(\{R_i\}_{i\in\Omega_\alpha}, \{R^0\})] \qquad (5)$$

$$n(RMSD) = \frac{1 - (RMSD/0.1)^8}{1 - (RMSD/0.1)^{12}} \qquad (6)$$

where, $\{R_i\}_{i \in \Omega_\alpha}$ is the coordinate of the set $\Omega_\alpha$ representing six-residue peptide stretch and $\{R^0\}$ is the same for an ideal α- helix. Finally the $f_H$ is obtained by dividing S by maximum no of possible six-residue-helical stretches in peptide, $S_{max}$.

$$f_H = \frac{S}{S_{max}} \qquad (7)$$

The time evolution of this helical fraction is calculated for different peptides in both free state and bound state with RBD and represented in Figure 6.

The helical fraction is plotted for all the peptides throughout the 1000 ns simulation in both free and RBD-bound states (Figure S4). The helicity of the free peptides decreases after ~500ns for the majority of the peptides although the extent varies depending on the stapling agent (Figure S4A). The partial unfolding of the ACE2_wt have been observed by Das *et al* in a recent experimental study.[56] The peptide with double lactam staple (ACE2_la-la) is capable of maintaining maximum helicity ($f_H \sim 1.0$) most of the time. For the ACE2_mutant system, the helicity is reduced to ~50 % leading to the partial unfolding of the peptide. The ACE2_al-al and ACE2_la-al are also stabilized in a conformation with ~60% helicity. However, the ACE_wt and ACE2_al-la maintain their helicity around 75 %. In the complex with RBD, most of the peptides maintain a higher degree of helicity (more than ~70 %) in the confinement of RBD binding pocket throughout 1000 ns except RBD+ACE2_al-al (Figure S4B). Similar to RMSF, a comparison of the helical fraction of the peptides in the uncomplexed state and complex with RBD will provide a better understanding of conformational switching upon binding. The $f_H$ for each peptide in their apo and complexed state are plotted together in Figure 6.
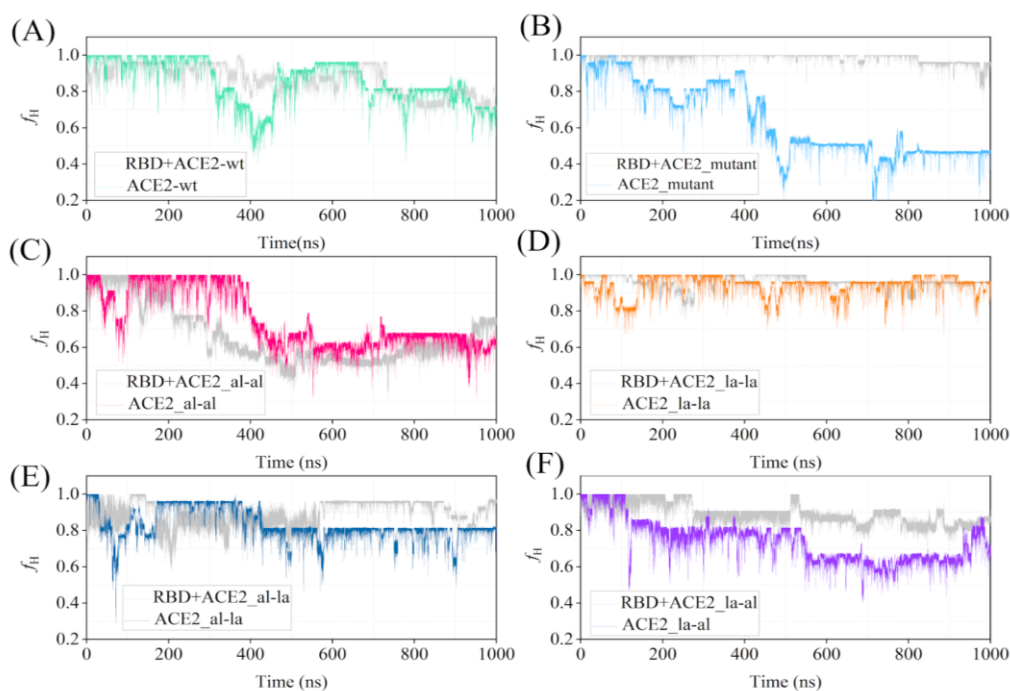
**Figure 6**: Comparison of time evolution helical fraction ($f_H$) of all ACE2 peptide variants in their free state and in complex with the receptor-binding domain (RBD). The helical fraction of the RBD-bound state is shown in gray in all the plots. The

From the plot of helical fraction, it is clear that $f_H$ of unstapled peptides decreases at the beginning of the simulation that is for ACE2_wt, it is dropped at 200 ns and then it fluctuated throughout the simulation whereas, for ACE2_mutant, decreases after 400 ns and peptide remained in a coiled conformation. Then, by adding lactam crosslinker as a stapling agent, the helical fraction of ACE2_la-la is maintained around 0.8 – 0.9 throughout the simulation but in the case of aliphatic crosslinker despite a stapling agent, helicity gets reduced after 400ns. This unexceptional behavior of ACE2_al-al could be explained based on the chemical nature of the stapling agent of the hydrophobic aliphatic chain. Similarly, for ACE2_al-la and ACE2_la-al, the helical fraction is maintained with a slight decrease in value during the simulation. Overall, lactam crosslinker is proved to be a good binder in maintaining the helicity of a long 25-mer peptide.

Furthermore, change in entropy of stapled designed peptides from complex to free state increases in comparison to hACE2_wt due to conformational restriction and rigidity of peptides by adding stapling agents both in the free and complex state. This is observed in the section of residue level fluctuation (RMSF) (Figure 5) and helicity (Figure 6) of peptides. Also, a helical conformation of peptide is suitable for binding with its target partner. Therefore, a comparison

of helicity of peptide in the free state and the bound state with RBD will give an idea of energy associated with conformational transition required by peptide to bind with RBD.

For ACE2_la-la, there is a great overlap of helicity value for ACE2_la-la and its bound state thus the transition from unbound state to bound state will require less amount of energy whereas, for the mutant system, they are quite apart. While considering the rest of the systems, slight overlap of helical fraction between free and complex states even though their helicity is decreased during the simulation. Considering all these facts, ACE2_al-la is proved to be a good binder with RBD of SARS-CoV-2.

## Discussion

Since the emergence of the global pandemic, there have been several attempts to design vaccines, antibodies, to combat viral attacks. Alongside that several efforts have been employed to design small molecule inhibitors which include both repurposing of clinically approved drugs or designing novel therapeutics.[16,57,58,59,60,61] At the same time, we have found the virus to mutate continuously to produce a large number of its variants some of which are found to be many times infectious than the original virus.[62,63,64] In this circumstance, it is important to understand the infection mechanism with structural detail and use that knowledge to design a more potent inhibitor. The strategy of designing peptide inhibitors takes the advantage of using some native protein-protein interactions responsible/necessary for the disease progression and using an effective shorter version of one of the partners involved in the PPI with modifications that enhance the binding affinity. In the present work, we have considered the interaction of spike protein of SARS Cov2 with human ACE2 receptor and designed some peptide inhibitors which can effectively bind to the receptor-binding domain of SARS-CoV-2 to inhibit them from binding to ACE2. The human ACE2 effectively interacts with the viral RBD through its α1 helix, more precisely the residue ranging from 21 to 45. This 25-residue domain has been considered as the starting structure (termed as ACE2_wt) and further modified to design a series of stapled peptides. A combination of two stapling agents (a hydrocarbon and a lactam stapling agent) has been used to design four stapled variants (Table 1). The detailed analyses of their binding mechanism to RBD in terms of different structural parameters and binding thermodynamics have revealed that the peptide with two lactam crosslinkers (ACE2_la-la) is the most effective inhibitor. The protein-peptide binding free energy is a sum of enthalpic and entropic components. The value of binding free energy provides a quantitative estimation of the energetic gain when the protein and the peptide combine to form a complex instead of being in their free state separately. Therefore, a proper

understanding of the binding mechanism in terms of binding free energy requires consideration of the ensemble of conformations of RBD and the ACE2-peptides in the free and bound state. There is a lack of these details in many protein-peptide binding energy estimation studies including the few that consider SRS-CoV2-ACE2 binding. For example, the estimated free energies for some variants of ACE2-peptide by de Campos *et al.* are in the range of -75 to -90 kcal/mol.[26] In their study they have not considered separate simulations for ACE2 and RBD and also the calculation of entropy is ignored. Similarly, Sitthiyota *et al.* have found MM-GBSA binding energy for some 25-residue ACE2-peptide with RBD to be in the range -50 to -70 kcal/mol which does not include entropy of binding.[29] Unlike those studies, we have considered separate simulations for both ACE2-peptides and RBD along with their complexes and entropy of binding has also been calculated. The outcome is a considerable range of binding free energy (-15 to -45 kcal/mol) and the change values of enthalpy and entropy can be correlated with structural modifications in the peptides. The dynamics of the truncated $\alpha1$ helix of ACE2 (ACE2_wt) at the binding pocket of RBD shows that the peptide does not bind in a fixed and stable orientation to the binding pocket rather it undergoes large reorientation to explore different orientations (Movie S1). During this process, it undergoes partial unfolding towards the C-terminal and N-terminal ends. The introduction of stapling agents to positions 28, 32, 36, and 40 improves the binding considerably. In the case of ACE2_al-al, the fluctuation of the N-terminal end of the peptide (21-30) has significantly decreased compared to ACE2_wt though the C-terminal end (30-45) shows deviation from strong association with RBD surface (Movie S2). This has been reflected in the RMSF (Figure 5C) and fraction helicity (Figure 6C) as well. Changing the stapling agent from aliphatic to lactam has further reduced this fluctuation (Figure 5D and 6D) and the ACE2_la-la anchors very well on the surface of RBD (Movie S3). This differences in the dynamics of the ACE2_peptides in complex with RBD and their associations with binding pocket residues of RBD have been reflected in the binding free energies which follows the order: $\Delta G_{RBD-ACE2\_la-la} < \Delta G_{RBD-ACE2\_al-al} < \Delta G_{RBD-ACE2\_wt}$ (Table 2). A deconvolution of the free energies into enthalpy and entropy reveals that the binding is guided by changes in both enthalpy ($\Delta H$) and entropy ($\Delta S$). Both ACE2_al-al and ACE2_la-la have improved $\Delta H$ (-51.5 and -55.28 kcal/mol respectively) than ACE2_wt (-40.31 kcal/mol). This enhancement in $\Delta H$ arises from the increase in salt-bridge interaction and hydrogen-bonded interaction of the polar amino acids of ACE2_al-al and ACE2_la-la with the amino acids at the RBD surface (Figure 4). A higher value of $-T\Delta S$ indicates higher entropic penalty which disfavors the binding. A comparison of $-T\Delta S$ of binding of ACE2_la-la (19.08 kcal/mol) to RBD compared to RBD-ACE2_wt (21.97 kcal/mol) and RBD-ACE2_mutant (27.83

kcal/mol) binding shows that introduction of a crosslinker by replacing hydrophobic residues (F28, F32, A36, and F40) or just simple lactamization of two Glu-Arg pairs (Glu28-Arg32, and Glu36-Arg40) reduces the entropic penalty. The reduction in the fluctuation of the free peptide and thereby a conformational similarity between the peptides in unbound and RBD-bound state has been reflected in the overlaps between RMSFs and fractions of helicity. The plots of RMSF and helical fraction of free and RBD-bound state together for different peptides shows considerable overlap between them for ACE2_la-la (Figure 5D and 6D) while they differ significantly for ACE2_wt (Figure 5A and 6A) and ACE2_mutant (Figure 5B and 6B). The impact of these overlaps has been reflected in the $-T\Delta S$ value (Table 2).

## Conclusion

Employing computational modeling and molecular dynamic simulation, we have developed an approach to design stapled peptide inhibitors derived from human ACE2 against the receptor-binding domain (RBD) of SARS-CoV-2. These peptides are designed to improve the binding affinity by forming new interactions with RBD in addition to the native RBD-ACE2 interactions. Starting from a 25-residue domain of the α1 helix of ACE2, a series of mutated and stapled ACE2 peptides have been designed by using a combination of aliphatic and lactam stapling agents. From the estimation of binding free energy, the ACE2 peptide with two lactam staples connected in the residue positions 28, 32, 36, and 40 is found to be the most promising one. The benefit of using a lactam stapling agent is two-fold. In the presence of the stapling agents, the RBD-ACE2 interactions get reorganized to enhance salt-bridge and hydrogen-bonded interaction which contributes to a more negative change in the enthalpy of binding. In addition to that, the stapling agents restrict the conformational flexibility of the free peptide and thereby reduce the change in entropy of going from a free to an RBD-bound state. To the best of our knowledge, this is the first study where the binding thermodynamics of RBD-ACE2 interaction have been fine-tuned by modulating the nature of the stapling agent to design a promising stapled peptide inhibitor against SARS-CoV-2. We believe that with experimental validation of the preferential binding of the designed peptide, this study will pioneer the rational designing of suitable inhibitors to combat the infection by SARS-CoV-2.

## Supplementary Information

Contact map between residues of RBD and ACE2-peptide for different systems; Snapshots from trajectory showing the hydrogen bonds between RBD and ACE2 residues; Root mean square fluctuation (RMSF) of different ACE2-peptides in the free state and in their complexes

with RBD; The helical fraction of different ACE2-peptides in free state and in their complexes with RBD; Details of energy components of the systems in multiple simulations; Movies showing the dynamics of ACE2_wt, ACE2_al-al and ACE2_la-la on the binding pocket of RBD.

## Author Information

**Corresponding Author**

*Email: rajarshi@chem.iitb.ac.in

Mailing Address: Department of Chemistry, Indian Institute of Technology Bombay, Powai, Mumbai-400076, India.

Phone: + 91-022-2576 7192.

Fax: + 91-022-2576 7152.

## Conflicts of Interest

The authors declare no competing financial interest.

## Acknowledgment

## References:

1       Weekly operational update on COVID-19 - 23 November 2021, https://www.who.int/publications/m/item/weekly-operational-update-on-covid-19---23-november-2021.

2       J. F. W. Chan, S. Yuan, K. H. Kok, K. K. W. To, H. Chu, J. Yang, F. Xing, J. Liu, C. C. Y. Yip, R. W. S. Poon, H. W. Tsoi, S. K. F. Lo, K. H. Chan, V. K. M. Poon, W. M. Chan, J. D. Ip, J. P. Cai, V. C. C. Cheng, H. Chen, C. K. M. Hui and K. Y. Yuen, A familial cluster of pneumonia associated with the 2019 novel coronavirus indicating person-to-person transmission: a study of a family cluster, *Lancet*, 2020, **395**, 514–523.

3       K. Kupferschmidt and J. Cohen, Will novel virus go pandemic or be contained?, *Science.*, 2020, **367**, 610–611.

4       Z. Abdelrahman, M. Li and X. Wang, Comparative Review of SARS-CoV-2, SARS-CoV, MERS-CoV, and Influenza A Respiratory Viruses, *Front. Immunol.*, 2020, **0**, 2309.

5       M. Shah, B. Ahmad, S. Choi and H. Goo, Mutations in the SARS-CoV-2 spike RBD

are responsible for stronger ACE2 binding and poor anti-SARS-CoV mAbs cross-neutralization, *Comput. Struct. Biotechnol. J.*, 2020, **18**, 3402–3414.

6    L. Fallon, K. A. A. Belfon, L. Raguette, Y. Wang, D. Stepanenko, A. Cuomo, J. Guerra, S. Budhan, S. Varghese, C. P. Corbo, R. C. Rizzo and C. Simmerling, Free Energy Landscapes from SARS-CoV-2 Spike Glycoprotein Simulations Suggest that RBD Opening Can Be Modulated via Interactions in an Allosteric Pocket, *J. Am. Chem. Soc.*, 2021, **143**, 11349–11360.

7    J. Lan, J. Ge, J. Yu, S. Shan, H. Zhou, S. Fan, Q. Zhang, X. Shi, Q. Wang, L. Zhang and X. Wang, Structure of the SARS-CoV-2 spike receptor-binding domain bound to the ACE2 receptor, *Nature*, 2020, **581**, 215–220.

8    A. Acharya, D. L. Lynch, A. Pavlova, Y. T. Pang and J. C. Gumbart, ACE2 glycans preferentially interact with SARS-CoV-2 over SARS-CoV, *Chem. Commun.*, 2021, **57**, 5949–5952.

9    A. Pavlova, Z. Zhang, A. Acharya, D. L. Lynch, Y. T. Pang, Z. Mou, J. M. Parks, C. Chipot and J. C. Gumbart, Machine Learning Reveals the Critical Interactions for SARS-CoV-2 Spike Protein Binding to ACE2, *J. Phys. Chem. Lett.*, 2021, **12**, 5494–5502.

10   I. Astuti, Severe Acute Respiratory Syndrome Coronavirus 2 (SARS-CoV-2): An overview of viral structure and host response, *Diabetes Metab. Syndr. Clin. Res. Rev.*, 2020, **14**, 407–412.

11   Y. Huang, C. Yang, X. feng Xu, W. Xu and S. wen Liu, *Acta Pharmacol. Sin.*, 2020, 41, 1141–1149.

12   M. I. Zimmerman, J. R. Porter, M. D. Ward, S. Singh, N. Vithani, A. Meller, U. L. Mallimadugula, C. E. Kuhn, J. H. Borowsky, R. P. Wiewiora, M. F. D. Hurley, A. M. Harbison, C. A. Fogarty, J. E. Coffland, E. Fadda, V. A. Voelz, J. D. Chodera and G. R. Bowman, SARS-CoV-2 simulations go exascale to predict dramatic spike opening and cryptic pockets across the proteome, *Nat. Chem. 2021 137*, 2021, **13**, 651–659.

13   Z. F. Brotzakis, T. Löhr and M. Vendruscolo, Determination of intermediate state structures in the opening pathway of SARS-CoV-2 spike using cryo-electron microscopy, *Chem. Sci.*, 2021, **12**, 9168–9175.

14   R. Yan, Y. Zhang, Y. Li, L. Xia, Y. Guo and Q. Zhou, Structural basis for the recognition of SARS-CoV-2 by full-length human ACE2, *Science.*, 2020, **367**, 1444–1448.

15   E. P. Barros, L. Casalino, Z. Gaieb, A. C. Dommer, Y. Wang, L. Fallon, L. Raguette, K. Belfon, C. Simmerling and R. E. Amaro, The flexibility of ACE2 in the context of SARS-CoV-2 infection, *Biophys. J.*, 2021, **120**, 1072–1084.

16   E. N. Muratov, R. Amaro, C. H. Andrade, N. Brown, S. Ekins, D. Fourches, O. Isayev, D. Kozakov, J. L. Medina-Franco, K. M. Merz, T. I. Oprea, V. Poroikov, G. Schneider, M. H. Todd, A. Varnek, D. A. Winkler, A. V. Zakharov, A. Cherkasov and A. Tropsha, A critical overview of computational approaches employed for COVID-19 drug discovery, *Chem. Soc. Rev.*, 2021, **50**, 9121–9151.

17   D. E. Scott, A. R. Bayly, C. Abell and J. Skidmore, Small molecules, big targets: drug discovery faces the protein--protein interaction challenge, *Nat. Rev. Drug Discov.*,

2016, **15**, 533–550.

18    M. Pelay-Gimeno, A. Glas, O. Koch and T. N. Grossmann, Structure-based design of inhibitors of protein--protein interactions: mimicking peptide binding epitopes, *Angew. Chem. Int. Ed.*, 2015, **54**, 8896–8927.

19    M. C. Smith and J. E. Gestwicki, Features of protein–protein interactions that translate into potent inhibitors: topology, surface area and affinity, *Expert Rev. Mol. Med.*

20    P. Wójcik and Ł. Berlicki, Peptide-based inhibitors of protein–protein interactions, *Bioorg. Med. Chem. Lett.*, 2016, **26**, 707–713.

21    F. Curreli, S. M. B. Victor, S. Ahmed, A. Drelich, X. Tong, C. T. K. Tseng, C. D. Hillyer and A. K. Debnath, Stapled peptides based on human angiotensin-converting enzyme 2 (Ace2) potently inhibit sars-cov-2 infection in vitro, *MBio*, 2020, **11**, e02451-20.

22    M. Klein, Stabilized helical peptides: overview of the technologies and its impact on drug discovery, *Expert. Opin. Drug. Discov.*, 2017, **12**, 1117–1125.

23    L. D. Walensky and G. H. Bird, Hydrocarbon-Stapled Peptides: Principles, Practice, and Progress Terms of Use, *J. Med. Chem*, 2014, **57**, 6275–6288.

24    Y. S. Tan, D. P. Lane and C. S. Verma, Stapled peptide design: principles and roles of computation, *Drug Discov. Today*, 2016, **21**, 1642–1653.

25    A. Das, A. Yadav, M. Gupta, P. R, V. L. Terse, V. Vishvakarma, S. Singh, T. Nandi, A. Banerjee, K. Mandal, S. Gosavi, R. Das, S. R. K. Ainavarapu and S. Maiti, Rational Design of Protein-Specific Folding Modifiers, *J. Am. Chem. Soc.*, 2021, **143**, 18766–18776.

26    L. J. de Campos, N. Y. Palermo and M. Conda-Sheridan,  Targeting SARS-CoV-2 Receptor Binding Domain with Stapled Peptides: An In Silico Study , *J. Phys. Chem. B*, 2021, **125**, 6572–6586.

27    M. N. Maas, J. C. J. Hintzen, P. M. G. Löffler and J. Mecinović, Targeting SARS-CoV-2 spike protein by stapled hACE2 peptides., *Chem. Commun. (Camb).*, 2021, **57**, 3283–3286.

28     and B. L. P. et al. G. Zhang, S. Pomplun, A. R. Loftis, X. Tan1, A. Loas, The first-in-class peptide binder to the SARS-CoV-2 spike protein, *bioarxiv*.

29    T. Sitthiyotha and S. Chunsrivirot, Computational Design of 25-mer Peptide Binders of SARS-CoV-2, *J. Phys. Chem. B*, 2020, **124**, 10930–10942.

30    P. Chaturvedi, Y. Han, P. Král and L. Vuković, Adaptive Evolution of Peptide Inhibitors for Mutating SARS-CoV-2, *Adv. Theory Simulations*, 2020, **3**, 2000156.

31    Y. Han and P. Král, Computational Design of ACE2-Based Peptide Inhibitors of SARS-CoV-2, *ACS Nano*, 2020, **14**, 5143–5147.

32    H. Othman, Z. Bouslama, J.-T. Brandenburg, J. da Rocha, Y. Hamdi, K. Ghedira, N. Srairi-Abid and S. Hazelhurst, Interaction of the spike protein RBD from SARS-CoV-2 with ACE2: similarity with SARS-CoV, hot-spot analysis and effect of the receptor polymorphism, *Biochem. Biophys. Res. Commun.*, 2020, **527**, 702–708.

33    R. B. Best, X. Zhu, J. Shim, P. E. M. Lopes, J. Mittal, M. Feig and A. D. MacKerell Jr,

Optimization of the additive CHARMM all-atom protein force field targeting improved sampling of the backbone φ, ψ and side-chain χ1 and χ2 Dihedral Angles, *J. Chem. Theory Comput.*, 2012, **8**, 3257–3273.

34    A. Maity, A. R. Choudhury and R. Chakrabarti, Effect of Stapling on the Thermodynamics of mdm2–p53 Binding, *J. Chem. Inf. Model.*, 2021, **61**, 1989–2000.

35    P. Mark and L. Nilsson, Structure and Dynamics of the TIP3P, SPC, and SPC/E Water Models at 298 K, *J. Phys. Chem. A*, 2001, **105**, 9954–9960.

36    S. S. Petrova and A. D. Solov'ev, The origin of the method of steepest descent, *Hist. Math.*, 1997, **24**, 361–375.

37    G. Bussi, D. Donadio and M. Parrinello, Canonical sampling through velocity rescaling, *J. Chem. Phys.*, 2007, **126**, 014101.

38    M. Parrinello and A. Rahman, Polymorphic transitions in single crystals: A new molecular dynamics method, *J. Appl. Phys.*, 1981, **52**, 7182–7190.

39    D. Spoel, E. Lindahl, B. Hess, G. Groenhof, A. E. Mark and H. J. C. Berendsen, GROMACS: fast, flexible, and free, *J. Comput. Chem.*, 2005, **26**, 1701–1718.

40    M. P. Allen and D. J. Tildesley, *Computer simulation of liquids: Second edition*, Oxford University Press, 2017.

41    H. C. Andersen, Rattle: A 'velocity' version of the shake algorithm for molecular dynamics calculations, *J. Comput. Phys.*, 1983, **52**, 24–34.

42    T. Darden, D. York and L. Pedersen, Particle mesh Ewald: An $N \cdot \log(N)$ method for Ewald sums in large systems, *J. Chem. Phys.*, 1993, **98**, 10089–10092.

43    W. Humphrey, A. Dalke and K. Schulten, VMD: Visual molecular dynamics, *J. Mol. Graph.*, 1996, **14**, 33–38.

44    I. Bill R. Miller, J. T. Dwight McGee, J. M. Swails, N. Homeyer, H. Gohlke and A. E. Roitberg, MMPBSA.py: An Efficient Program for End-State Free Energy Calculations, *J. Chem. Theory Comput.*, 2012, **8**, 3314–3321.

45    D. Sitkoff, K. A. Sharp and B. Honig, Accurate Calculation of Hydration Free Energies Using Macroscopic Solvent Models, *J. Phys. Chem.*, 1994, **98**, 1978–1988.

46    Chunhu Tan, A. Yu-Hong Tan and R. Luo, Implicit Nonpolar Solvent Models, *J. Phys. Chem. B*, 2007, **111**, 12263–12274.

47    S. Genheden and U. Ryde, The MM/PBSA and MM/GBSA methods to estimate ligand-binding affinities, *Expert Opin. Drug Discov.*, 2015, **10**, 449–461.

48    B. R. Brooks, D. Janežič and M. Karplus, Harmonic analysis of large systems. I. Methodology, *J. Comput. Chem.*, 1995, **16**, 1522–1542.

49    A. D. Mackerell, M. Feig and C. L. Brooks, Extending the treatment of backbone energetics in protein force fields: Limitations of gas-phase quantum mechanics in reproducing protein conformational distributions in molecular dynamics simulation, *J. Comput. Chem.*, 2004, **25**, 1400–1415.

50    P. A. Greenidge, C. Kramer, J. C. Mozziconacci and R. M. Wolf, MM/GBSA binding energy prediction on the PDBbind data set: Successes, failures, and directions for

further improvement, *J. Chem. Inf. Model.*, 2013, **53**, 201–209.

51    S. G. Dastidar, D. P. Lane and C. S. Verma, Multiple peptide conformations give rise to similar binding affinities: Molecular simulations of p53-MDM2, *J. Am. Chem. Soc.*, 2008, **130**, 13514–13515.

52    S. Kumar and R. Nussinov, Close-Range Electrostatic Interactions in Proteins, *ChemBioChem*, 2002, **3**, 604–617.

53    A. Aggarwal, S. Naskar, N. Maroli, B. Gorai, N. M. Dixit and P. K. Maiti, Mechanistic insights into the effects of key mutations on SARS-CoV-2 RBD–ACE2 binding, *Phys. Chem. Chem. Phys.*, 2021, **23**, 26451–26458.

54    M. Bonomi, D. Branduardi, G. Bussi, C. Camilloni, D. Provasi, P. Raiteri, D. Donadio, F. Marinelli, F. Pietrucci, R. A. Broglia and M. Parrinello, PLUMED: A portable plugin for free-energy calculations with molecular dynamics, *Comput. Phys. Commun.*, 2009, **180**, 1961–1972.

55    F. Pietrucci and A. Laio, A Collective Variable for the Efficient Exploration of Protein Beta-Sheet Structures: Application to SH3 and GB1, *J. Chem. Theory Comput.*, 2009, **5**, 2197–2201.

56    A. Das, V. Vishvakarma, A. Dey, S. Dey, A. Gupta, M. Das, K. K. Vishwakarma, D. S. Roy, S. Yadav, S. Kesarwani, R. Venkatramani and S. Maiti, Biophysical properties of the isolated spike protein binding helix of human ACE2, *Biophys. J.*, 2021, **120**, 2785–2792.

57    N. Vithani, M. D. Ward, M. I. Zimmerman, B. Novak, J. H. Borowsky, S. Singh and G. R. Bowman, SARS-CoV-2 Nsp16 activation mechanism and a cryptic pocket with pan-coronavirus antiviral potential, *Biophys. J.*, 2021, **120**, 2880–2889.

58    A. Acharya, R. Agarwal, M. B. Baker, J. Baudry, D. Bhowmik, S. Boehm, K. G. Byler, S. Y. Chen, L. Coates, C. J. Cooper, O. Demerdash, I. Daidone, J. D. Eblen, S. Ellingson, S. Forli, J. Glaser, J. C. Gumbart, J. Gunnels, O. Hernandez, S. Irle, D. W. Kneller, A. Kovalevsky, J. Larkin, T. J. Lawrence, S. Legrand, S. H. Liu, J. C. Mitchell, G. Park, J. M. Parks, A. Pavlova, L. Petridis, D. Poole, L. Pouchard, A. Ramanathan, D. M. Rogers, D. Santos-Martins, A. Scheinberg, A. Sedova, Y. Shen, J. C. Smith, M. D. Smith, C. Soto, A. Tsaris, M. Thavappiragasam, A. F. Tillack, J. V. Vermaas, V. Q. Vuong, J. Yin, S. Yoo, M. Zahran and L. Zanetti-Polzi, Supercomputer-Based Ensemble Docking Drug Discovery Pipeline with Application to Covid-19, *J. Chem. Inf. Model.*, 2020, **60**, 5832–5852.

59    S. J. Adrian Mulholland, G. M. Morris, S. eld, H. T. Henry Chan, M. A. Moesser, R. K. Walters, cd R. Tika Malla, R. M. Twidale, T. John, H. M. Deeks, cd Tristan Johnston-Wood, V. Mikhailov, R. B. Sessions, W. Dawson, E. Salah, P. Lukacik, gh Claire Strain-Damerell, gh C. David Owen, gh Takahito Nakajima, K. Swiderek, A. Lodola, V. Moliner, D. R. Glowacki, J. Spencer, M. A. Walsh, gh J. Christopher Schofield, L. Genovese, D. K. Shoemark, A. J. Mulholland and F. Duarte, Discovery of SARS-CoV-2 Mpro peptide inhibitors from modelling substrate and ligand binding, *Chem. Sci.*, 2021, **12**, 13686–13703.

60    R. Mao, L. Bie, M. Xu, X. Wang and J. Gao, Antiviral drug design based on the opening mechanism of spike glycoprotein in SARS-CoV-2, *Phys. Chem. Chem. Phys.*, 2021, **23**, 12549–12558.

61    A. A. A. A. Abu-Saleh, I. E. Awad, A. Yadav and R. A. Poirier, Discovery of potent inhibitors for SARS-CoV-2's main protease by ligand-based/structure-based virtual screening, MD simulations, and binding energy calculations, *Phys. Chem. Chem. Phys.*, 2020, **22**, 23099–23106.

62    A. Triveri, S. A. Serapian, F. Marchetti, F. Doria, S. Pavoni, F. Cinquini, E. Moroni, A. Rasola, F. Frigerio and G. Colombo, SARS-CoV-2 Spike Protein Mutations and Escape from Antibodies: A Computational Model of Epitope Loss in Variants of Concern, *J. Chem. Inf. Model.*, 2021, **61**, 4687–4700.

63    C. Bai, J. Wang, G. Chen, H. Zhang, K. An, P. Xu, Y. Du, R. D. Ye, A. Saha, A. Zhang and A. Warshel, Predicting Mutational Effects on Receptor Binding of the Spike Protein of SARS-CoV-2 Variants, *J. Am. Chem. Soc.*, 2021, **143**, 17646–17654.

64    J. Chen, K. Gao, R. Wang and G. W. Wei, Prediction and mitigation of mutation threats to COVID-19 vaccines and antibody therapies, *Chem. Sci.*, 2021, **12**, 6929–6948.

**Table of Content Graphics**